Astron. Astrophys. 279, 615–626 (1993)

ASTRONOMY AND ASTROPHYSICS

Atmospheric fragmentation of meteoroids

Z. Ceplecha, P. Spurný, J. Borovička, and J. Keclíková

Astronomical Institute of the Academy of Sciences of the Czech Republic, 251 65 Ondřejov Observatory, The Czech Republic

Received March 9, accepted April 24, 1993

Abstract. The single body theory of meteoroid interaction with the atmosphere in the form of $l = l(t)$, where l is the relative distance along the meteoroid trajectory and t the relative time, is generalized by allowing for points of sudden gross-fragmentation. This theory can be directly applied to photographic observations of meteors, comparing the measured distance, l_{obs}, with the model computed distance, l, by means of the least-squares method. The no-fragmentation case has 4 free parameters to be determined from observations ($l_0, v_0, v_\infty, \sigma$), distance and velocity at time $t = 0$, velocity at $t = -\infty$ and ablation coefficient, respectively. The case of one gross-fragmentation point adds two more free parameters to the problem, $v_{\infty 2}$ and σ_2, velocity at $t = -\infty$ and ablation coefficient, both for the second part of the trajectory after fragmentation. Moreover the position of the gross-fragmentation point and relative amount of fragmented mass can also be determined from photographic observations by searching for the best fit for different choices of the fragmentation point. The single body model applied to theoretically computed data for a meteoroid with fragmentation points enabled insight into time dependence of residuals, their relation to position of fragmentation point and influence on the resulting ablation coefficient, initial velocity and mass. Moreover, the model was checked by means of 11 PN (Prairie Network) photographs, where the splitting into individual fragments was directly visible and the fragmentation point has been determined geometrical way from intersections of trajectories of individual fragments. A computer program for automatic search of gross-fragmentation points was applied to 80 records of PN fireballs. Fireballs can be separated according to their sudden fragmentation into NF (no-fragmentation), 1F (one fragmentation point), MF (many fragmentation points) and LA (low accuracy, cannot decide) classes. The dynamic pressure ρv^2 (ρ the air density) at the fragmentation points of 1F and MF fireballs tends to cluster at several separate values. This is used for proposing a classification into several strength categories (a: 0.8 Mdyn/cm^2, b: 2.5, c: 5.3, d: 8.0, e: 11). The ablation ability groups I, II, IIIA and IIIB proposed earlier and these new proposed strength categories form a possibility of two dimensional classification for 1F and MF fireballs separating meteoroid composition and structure. Ablation coefficients proved to be lower than the previously determined statistical values, while the bulk densities are approximately the same as statistically determined. Ablation coefficients determined for meteoroids with gross-fragmentation are half of the values, which would result for the same fireball without taking the fragmentation effect into consideration. Gross-fragmentation at a point is more frequent for stronger types of fireballs. Typical amount of fragmented mass at the fragmentation point for 1F and MF fireballs is 60%. 1F fireballs have another typical value of the amount of fragmented mass, i.e. between 95% and 99%, which corresponds to almost complete disruption of the body. Initial velocities and masses for 1F and MF fireballs have to be determined by means of our model: their values without taking the gross-fragmentation effect into account are significantly different. We give also list of classified fireballs containing all PN fireballs, to which we applied our model. We discuss also precision of our results with special attention to the Lost City fireball. Our method needs very precise fireball records. PN fireballs are the most precise data available, but fulfill our requirements only partly. Thus we propose some remeasuring of the PN films, but mainly a new observing program by using cameras, which would yield fireball records with precision of several meters in distances along the trajectory.

Key words: meteoroids

1. Theoretical model

Multi-station (or double-station) photographs of fireballs are the most precise records of the meteoroid motion and ablation we possess for detailed comparison of our theoretical concepts with reality (McCrosky & Ceplecha 1969). For each time mark t (independent variable), our information from photographic multistation records contains $l_{\rm obs}$, distance flown by the meteoroid in its trajectory, $h_{\rm obs}$, the height above the Earth's surface, and $M_{\rm obs}$, stellar magnitude computed for 100 km distance, i.e. the absolute magnitude.

The motion and ablation of a single non-fragmenting body through the atmosphere is usually represented by three differential equations (Pecina & Ceplecha 1983, 1984): drag Eq. (1),

Send offprint requests to: Z. Ceplecha

mass-loss Eq. (2) and height Eq. (3), which is a purely geometrical one and is written here for a spherical Earth's surface, i.e. with cos z as a function of time.

$$\frac{dv}{dt} = -\Gamma A \varrho_d^{-2/3} \varrho m^{-1/3} v^2 \qquad (1)$$

$$\frac{dm}{dt} = -\frac{\Lambda A}{2\xi} \varrho_d^{-2/3} \varrho m^{2/3} v^3 \qquad (2)$$

$$\frac{dh}{dt} = \frac{l - A/2}{B/2 + h} v \qquad (3)$$

$$\frac{A/2 - l}{B/2 + h} = \cos z(t) \qquad (4)$$

$$Al + Bh + C = l^2 - h^2 \qquad (5)$$

Equation (5) contains constant values A, B, C, which are given by the geometrical relation between distances along the meteoroid trajectory and heights measured from the spherical Earth's surface. Equation (5) can also be used as a check of validity of any published l and h values on photographic meteors.

For a meteoroid at an arbitrary point of its trajectory, the notation has the following meaning: v ... velocity; t ... time (independent variable); m ... mass; h ... height; l ... distance along the trajectory; ϱ ... air density; z ... zenith distance of the radiant (inclination of the trajectory to the vertical); Γ ... drag coefficient; Λ ... heat transfer coefficient; A ... shape factor $A = Sm^{-2/3}\varrho_d^{2/3}$; S ... head cross-section; ϱ_d ... bulk density; ξ ... energy necessary for ablation of a unit mass. Two independent parameters of the problem can be expressed

$$\text{the ablation coefficient} \quad \sigma = \frac{\Lambda}{2\xi\Gamma} \qquad (6)$$

$$\text{the shape-density coefficient} \quad K = \Gamma A \varrho_d^{-2/3} \qquad (7)$$

Keeping σ and K constant, we can derive the following integrals of Eqs. (1), (2) and (3):

$$m = m_\infty \exp(\tfrac{1}{2}\sigma[v^2 - v_\infty^2]) \qquad (8)$$

where $m \to m_\infty$, $v \to v_\infty$, for $t \to -\infty$ (outside the atmosphere); the velocity integral by substitution of (8) into (1) and integrating,

$$\mathrm{Ei}(\tfrac{1}{6}\sigma v_\infty^2) - \mathrm{Ei}(\tfrac{1}{6}\sigma v^2) = \frac{2K \exp(\frac{1}{6}\sigma v_\infty^2)}{m_\infty^{1/3}} \int_h^\infty \frac{(B/2+h)\varrho\, dh}{(A^2/4 + C + h^2 + Bh)^{1/2}}; \qquad (9)$$

the integral relating velocity to time

$$t - t_0 = \int_{l_0}^{l} \frac{dl}{v}; \qquad (10)$$

and the integral relating height and distance along the trajectory to time

$$\frac{\mathrm{Ei}(\frac{1}{6}\sigma v_\infty^2) - \mathrm{Ei}(\frac{1}{6}\sigma v^2)}{\mathrm{Ei}(\frac{1}{6}\sigma v_\infty^2) - \mathrm{Ei}(\frac{1}{6}\sigma v_0^2)} = \frac{\int_h^\infty \frac{(B/2+h)\varrho\, dh}{(A^2/4+C+h^2+Bh)^{1/2}}}{\int_{h_0}^\infty \frac{(B/2+h)\varrho\, dh}{(A^2/4+C+h^2+Bh)^{1/2}}}, \qquad (11)$$

where the relation of height to distance is given by

$$h = -B/2 + \sqrt{B^2/4 - C + l^2 - Al}. \qquad (12)$$

Here $\mathrm{Ei}(x)$ is the exponential integral function, given by

$$\mathrm{Ei}(x) = \int_{-\infty}^{x} \frac{e^x}{x}\, dx, \qquad (13)$$

v is defined by (10) and $v = v_0$, $h = h_0$, $l = l_0$ holds for $t = t_0$. We define $t_0 = 0$ as the first measured rotating shutter break at which we start to count the relative time t.

These integrals hold for any air density profile. The Eqs. (10) and (11) represent the complete solution of the problem of the single no-fragmenting body and give the distance along the trajectory and the height for any chosen time, if the four parameters, l_0, v_0, v_∞, σ, are known. We can consider velocity, v, as an intermediate parameter to be eliminated from between the Eqs. (10) and (11). The solution (10) and (11) implies the condition K = constant.

The problem contains 4 unknown parameters l_0, v_0, v_∞, σ, to be determined from observations. We can make the problem linear by writing it for small increments of the parameters. The partial derivatives of (10) and (11) with respect to all four unknown parameters are explicit analytical expressions, as follows. This makes the computation quite quick, especially if we have some good estimates of the initial values of the parameters. We proceed by writing the total differential according to changing parameters, making thus the problem linear in computation of small increments of the unknown parameters.

$$l_{\mathrm{obs}} - l = \frac{\partial l}{\partial l_0}\Delta l_0 + \frac{\partial l}{\partial v_0}\Delta v_0 + \frac{\partial l}{\partial v_\infty}\Delta v_\infty + \frac{\partial l}{\partial \sigma}\Delta\sigma \qquad (14)$$

$$\frac{\partial l}{\partial l_0} = \frac{1}{v_0 D}\left\{2v \exp(\tfrac{1}{6}\sigma v^2)\int_{h_0}^\infty \frac{\varrho\, dh}{\cos z} + v_0 v^2[\mathrm{Ei}(\tfrac{1}{6}\sigma v_\infty^2) - \mathrm{Ei}(\tfrac{1}{6}\sigma v^2)]\varrho(h_0)\int_{l_0}^{l}\frac{dl}{v^2}\right\} \qquad (15)$$

$$\frac{\partial l}{\partial v_0} = \frac{2v^2}{v_0 D}\exp(\tfrac{1}{6}\sigma v_0^2)\int_h^\infty \frac{\varrho\, dh}{\cos z}\int_{l_0}^{l}\frac{dl}{v^2} \qquad (16)$$

$$\frac{\partial l}{\partial v_\infty} = -\frac{2v^2}{v_\infty D}\exp(\tfrac{1}{6}\sigma v_\infty^2)\left[\int_h^\infty \frac{\varrho\, dh}{\cos z} - \int_{h_0}^\infty \frac{\varrho\, dh}{\cos z}\right]\int_{l_0}^{l}\frac{dl}{v^2} \qquad (17)$$

$$\frac{\partial l}{\partial \sigma} = \frac{v^2}{\sigma D}\int_{l_0}^{l}\frac{dl}{v^2}\left[\exp(\tfrac{1}{6}\sigma v_0^2)\int_h^\infty \frac{\varrho\, dh}{\cos z} - \exp(\tfrac{1}{6}\sigma v_\infty^2)\int_h^{h_0}\frac{\varrho\, dh}{\cos z} - \exp(\tfrac{1}{6}\sigma v^2)\int_h^\infty \frac{\varrho\, dh}{\cos z}\right] \qquad (18)$$

where the denominator D is given by

$$D = 2\exp(\tfrac{1}{6}\sigma v^2)\int_{h_0}^\infty \frac{\varrho\, dh}{\cos z} + v^2[\mathrm{Ei}(\tfrac{1}{6}\sigma v_\infty^2) - \mathrm{Ei}(\tfrac{1}{6}\sigma v_0^2)]\varrho(h)\int_{l_0}^{l}\frac{dl}{v^2} \qquad (19)$$

When this model was applied to observations of PN (Prairie Network) and EN (European Network) fireballs, the first inspection of changing signs of residuals revealed that at least one quarter of the cases displayed a systematic course of residuals with time (Ceplecha & Borovička 1992). Because continuous fragmentation is already contained in the definition of ablation coefficient in the single-body model, we suspected the only process, which is strong enough and may be responsible for systematic change of residuals with time: gross-fragmentation, i.e. a sudden, instantaneous breakage of the meteoroid. After the gross-fragmentation point, only the largest piece could be followed and measured on meteor photographs. This is the reason, why we worked out more general model containing a gross-fragmentation point. The simplest model with only one fragmentation point, is practically the same as given by Eqs. (10) and (11), except we have two parameters more to be determined from observations, i.e. altogether 6. If the gross-fragmentation point is located at $t = t_0$ (we can choose this point, from where the relative time is counted), then

$$l_{\mathrm{obs}} - l = \tag{20}$$
$$= \frac{\partial l}{\partial l_0}\Delta l_0 + \frac{\partial l}{\partial v_0}\Delta v_0$$
$$+ \frac{\partial l}{\partial v_{\infty 1}}\Delta v_{\infty 1} + \frac{\partial l}{\partial \sigma_1}\Delta \sigma_1 + \frac{\partial l}{\partial v_{\infty 2}}\Delta v_{\infty 2} + \frac{\partial l}{\partial \sigma_2}\Delta \sigma_2$$

which is a linear equation analogical to (14), except it contains the following 6 unknown increments of parameters to be determined from observation

$\Delta v_{\infty 1}, \Delta \sigma_1$	$\Delta l_0, \Delta v_0$	$\Delta v_{\infty 2}, \Delta \sigma_2$
before fragmentation	at fragmentation	after fragmentation

Partial derivatives in (20) are again explicit analytical expressions as in the no-fragmentation case (14), in complete analogy. Equation (17) and Eq. (18) are now written with two subscripts, 1 and 2: subscript 1 is valid before the fragmentation point and subscript 2 is valid after the fragmentation point. The computation procedure is analogical to that described above eq. (14). Because the solution is again completely equivalent to K = constant, the relative change of mass at the fragmentation point forms also a part of the solution. The ratio of $Km^{-1/3}$ before and after the fragmentation point determines m_f, the ratio of mass after and before the fragmentation point, which is independent of the actual value of K.

If we try all measured points as fragmentation points, different standard deviations of solutions result. If there is a minimum value among these solutions (they are expressed as function of time of the assumed fragmentation point) and if this minimum value is significantly lower than the solution without fragmentation (lower by one standard deviation of its standard deviation), the fragmentation point is considered to occur at this point (Fig. 1). Thus the complete solution has 8 unknown parameters: the 6 unknowns directly contained in the equations, the amount of fragmentation (relative percent of stripped-off mass) and the position of the fragmentation point.

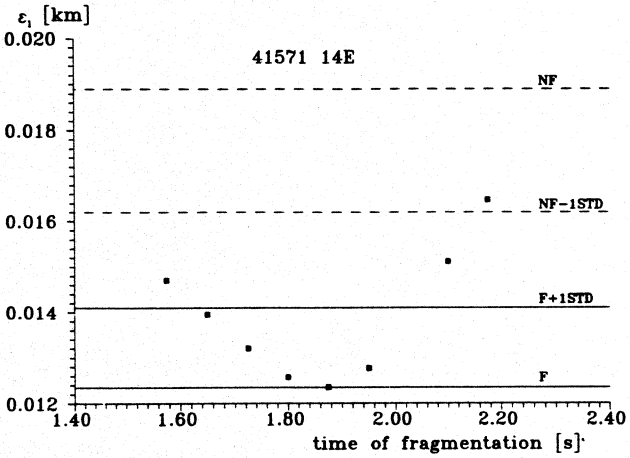

Fig. 1. Solution for gross-fragmentation point: ε_l ... standard deviation for one measured value (one time mark) is plotted against assumed time of the fragmentation point. The no-fragmentation solution (NF) is represented by the upper dashed line: the lower dashed line belongs to this NF solution minus one of its standard deviation. The lower full line belongs to the lowest ε_l found for fragmentation solutions, the upper full line is by one of its standard deviation higher. The condition we used for saying we have a significant solution: *F should be lower than* $NF - 1$. The minimum at F determines then time of the fragmentation point. The field of the other points, when it crosses the F+1STD level, determines the standard deviation of this fragmentation instant

Because we put no limitation on the change of mass at the fragmentation point, our solutions may also add mass to the body instead of its fragmentation. We call such solutions "inverse" fragmentation; they are of course physically unrealistic. The reason we also deal with "inverse" fragmentation solutions in this paper is simple: they sometimes yield better least squares fits than the fragmentation solutions; and in case of PN 40116, one of the splitting fireballs (Table 1), a very good "inverse" fragmentation solution was the only one we were able to find. We feel that these unrealistic solutions may hide some other, still unrecognized, effects.

In case of more fragmentation points, the situation is not so simple. Numerical differentiation is one possibility, separation of the fireball trajectory into several parts with independent solutions performed for each of these parts is another (which we actually used for the Lost City fireball). In any case solutions for more fragmentation points are possible only for very long and precisely determined fireball trajectories. In principle each fragmentation point adds four more parameters to be determined from observations, if the relative amount of fragmented mass and the position of fragmentation points are also taken as unknowns.

Table 1. No-fragmentation model (l_{com}) applied to theoretically computed (simulated) fireball (l_{obs}) with differently chosen position of the gross-fragmentation point. Assumption on the fragmented mass: 87% at the given points (at 0.25, 0.50 and 0.75 of the entire trajectory counting from its beginning on). ε_l is the standard deviation in the distance along the trajectory for one simulated measurement

	σ [s^2/km^2]	$Km_\infty{}^{-1/3}$ [c.g.s.]	v_∞ [km/s]	ε_l [m]
assumed	0.0151	0.0513	14.3343	0
fragmen. point at				
0.25	0.0171 ±.0002	0.0985 ±.0002	14.4528 ±.0013	±11
0.50	0.0353 ±.0008	0.0726 ±.0004	14.4680 ±.0052	±44
0.75	0.0605 ±.0004	0.0434 ±.0001	14.2886 ±.0023	±19

2. Verification of the model

2.1. Theoretical fireballs

The impact of gross fragmentation process on solutions performed with the no-fragmentation model was tested the following way proposed by McCrosky. First, theoretical distances and heights were computed for many time instants assuming for each case that gross-fragmentation occurred at a prechosen point of the meteoroid trajectory (time instants imitate the rotating shutter time marks). Different velocities of the meteoroid, different position of the fragmentation point and different relative quantity of the fragmented mass were assumed. The resulting theoretical meteoroid trajectory with the a priori known (chosen) position and intensity of fragmentation was analyzed by the no-fragmentation model. The non-zero residuals of solutions and their time dependence were the clue for understanding the problem. The main result may be expressed: time-dependent residuals of solutions with the no-fragmentation model may originate from the not-accounted-for gross-fragmentation. *Any systematic change of residuals with time exceeding one standard deviation may be caused by gross fragmentation.* As an example we present here residuals of solutions for a 14 km/s case with fragmentation point located at 0.25, 0.5 and 0.75 of the meteor trajectory (Fig. 2, Table 1).

The mass computed from the no-fragmentation model applied to the gross-fragmentation case with the fragmentation point close to the beginning of the trajectory is about one order of magnitude less than the mass assumed. Thus also the bulk density of the meteoroid without accounting for gross-fragmentation effect is usually lower than the reality, and in case of early fragmentation, even much lower. On the other hand, the resulting ablation coefficient behaves just opposite to mass. The gross-fragmentation located at the beginning of the trajectory does not greatly disturb the resulting ablation coefficient, but it does significantly affect the resulting dynamic mass and initial

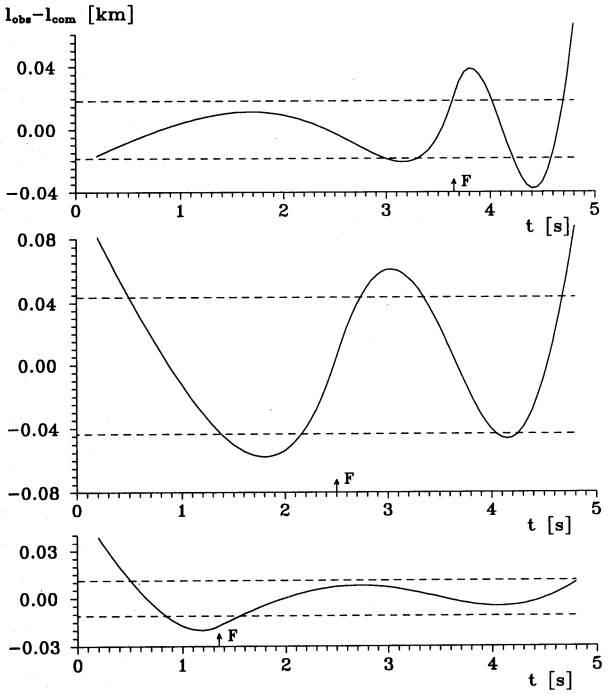

Fig. 2. Time dependence of residuals, when the no-fragmentation model is applied to a fireball with one-fragmentation point assumed. F ... fragmentation point. For parameters resulting from the least-squares solution see Table 1. Dashed lines are the standard deviation limits. $l_{com} \equiv l$

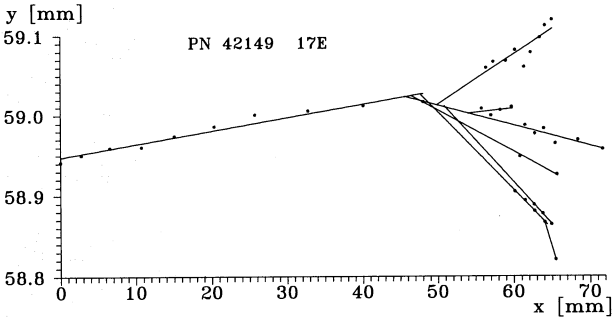

Fig. 3. Splitting trails of fireball PN 42149. This is the direct image as seen on the film except the y-axis is greatly enlarged to visualize separation of individual fragments. Dots are the directly measured points: least squares fits of straight lines to these points define trails of individual fragments. The main trail is terminated at the largest x

velocity. The gross-fragmentation point located at the end of the trajectory has the opposite effect on these parameters.

When the theoretical meteoroid trajectory with a single prechosen fragmentation point was analyzed by means of our fragmentation model, we received back the assumed values of σ, $Km_\infty{}^{-1/3}$, v_∞ exactly (e.g. the first row of Table 1). Also the assumed fragmentation point and relative amount of the fragmented mass (87% in case of Table 1) came out exactly as prechosen and the random errors resulted in standard deviation $\varepsilon_l = 0$. This was not only a good check of our model, but also a

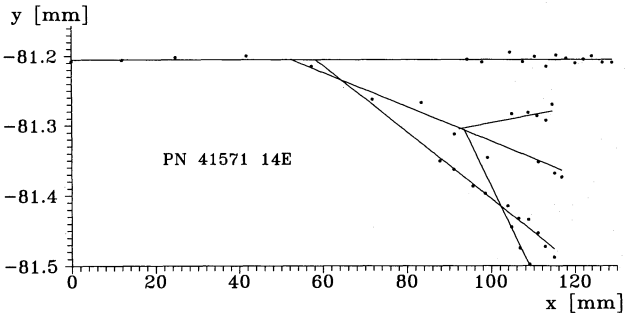

Fig. 4. Splitting trails of fireball PN 41571: explanations see Fig. 3

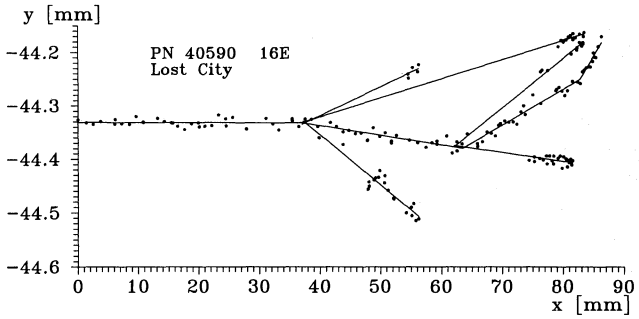

Fig. 5. Splitting trails of fireball PN 40590 (Lost City): explanations see Fig. 3

safe verification of the corresponding computer program used to search for fragmentation points automatically. Thus we proved that our model works *in the absence of random errors*. In the next subsection we will inspect the influence of random errors of measured distances on applicability of our method to observed fireballs.

2.2. *Photographic records of fireball splitting*

There is one strong possibility to check the gross-fragmentation model with random errors of measurements present: photographic records of fireballs with good visible splitting of trajectories belonging to individual fragments. We can measure trails of different fragments and by intersecting them we can determine the position of the break-up by this quite independent geometrical way. We can then compare the geometric position of the gross-fragmentation point with the position determined dynamical way from our model on assumption that, after fragmentation point, we see only the trajectory of the main piece. In this respect the PN records are preferable to EN and MORP (Meteorite Observation and Recovery Project, Canada) photographs because of longer focal distances of cameras (McCrosky et al. 1977), better recognition of the splitting trails and better precision of measured distances along the trajectory.

The rich collection of PN films at SAO contains many fireballs with trails of different fragments well visible. Here we give results for several of them in Table 2. As an example of how the geometrical intersections look like on the original photographs, we present here the situation for PN 42149 (Fig. 3), PN 41571

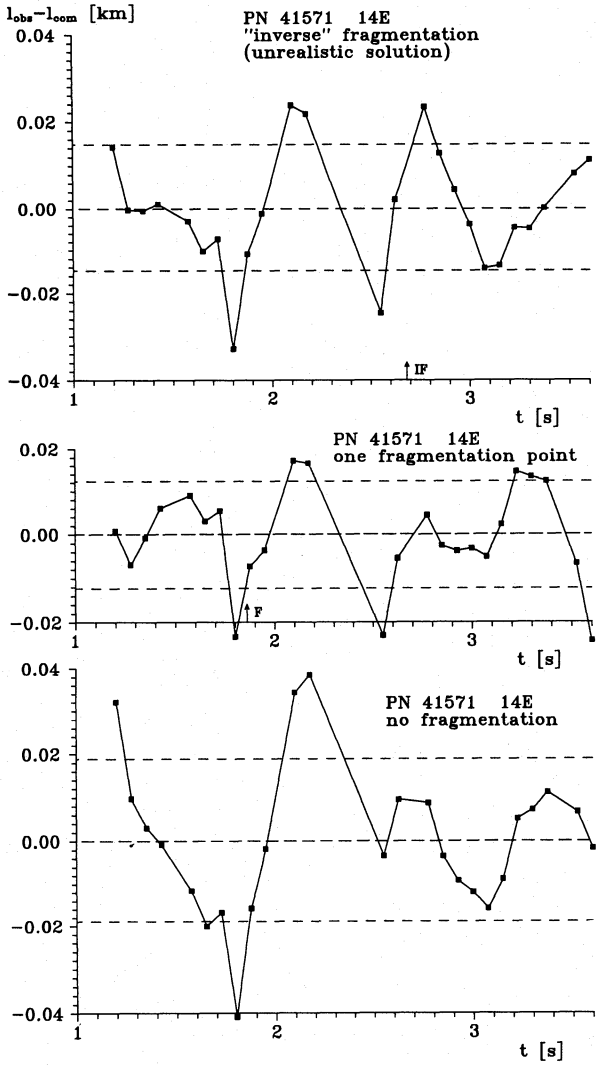

Fig. 6. PN 41571: Comparison of time dependence of residuals from the single body-solution with residuals from our model solution. $l_{com} \equiv l$

(Fig. 4) and for Lost City fireball (PN 40590 in Fig. 5). In order to visualize also the improvement of residuals, we present here comparison of time dependence of residuals for single-body solution and for our model solution for three fireballs (Fig. 6, Fig. 7, Fig. 8) including the unrealistic "inverse" solutions.

In case we could also apply our method to individual fragments and make independent solutions, we checked our model one other way. As an example we present here an independently derived velocity for the main body and the main fragment of fireball PN 41571 (Fig. 9).

All measurements were done by one of us (Keclíková) at the Ondřejov Observatory using Zeiss Ascorecord device with our own software evaluation. After tedious work of recognizing and measuring patterns in the maze of abundant fragment trails on PN fireball records, after applying our theoretical model of section 1 to make independent dynamic analyses of the fragmentation points, and after comparing these "geometric" and "dynamic" fragmentation points (Table 2), we can make sev-

Table 2. Comparison of fragmentation points determined geometrical way from fireball trail splitting with dynamical solution for them from our model

fireball No. PN	fragmentation: geometrical solution t_{f1} [s]	t_{f2} [s]	t_{f3} [s]	t_{f4} [s]	fragmentation: dynamical solution t_f [s]	m_f %	σ [s^2/km^2]	ε_l [m]	"inverse" fragmentation t_{if} [s]	σ_{if} [s^2/km^2]	ε_l [m]	single body no fragmentation σ [s^2/km^2]	ε_l [m]
39404	2.11 ±.06	2.62 ±.06	3.66 ±.09	–	3.77 ±.16	59 ±6	0.012 ±.002	±18	–	–	–	0.0255 ±.0004	±20
39972	2.54 ±.10	3.19 ±.04	–	–	3.2 ±.1	87 ±5	0.007 ±.001	±53	1.95 ±.30	0.027 ±.001	±42	0.0146 ±.0008	±61
40116[a]	2.16 ±.01	2.77 ±.01	–	–	–	–	–	–	2.4 ±.2	0.100 ±.004	±34	0.004 ±.003	±41
40590[b] Lost City	5.35 ±.01	6.65 ±.06	8.30 ±.07	–	5.1 ±.7	60 ±2	0.0163 ±.0003	±23	7.10 ±.08	0.039 ±.002	±24	0.0216 ±.0003	±32
40617	5.24 ±.04	5.87 ±.03	6.35 ±.03	6.85 ±.02	7.4 ±.5	35 ±3	0.022 ±.002	±29	3.9 ±.9	0.0315 ±.0004	±28	0.0281 ±.0003	±31
41126	2.17 ±.07	2.9 ±.4	–	–	3.5 ±.2	68 ±4	0.0071 ±.0002	±22	2.7 ±.2	0.0115 ±.0003	±22	0.0084 ±.0002	±33
41327[c]	1.82 ±.11	2.42 ±.07	4.02 ±.03	–	3.7 ±.3	90 ±2	0.006 ±.002	±12	4.7 ±.1	0.136 ±.003	±9	0.042 ±.002	±26
41571 (Fig. 4)	1.91 ±.04	–	–	–	1.86 ±.21	64 ±2	0.0119 ±.0003	±12	2.68 ±.12	0.023 ±.001	±15	0.0141 ±.0002	±19
41963	−0.78 ±.14	1.50 ±.02	2.06 ±.02	–	2.09 ±.12	77 ±3	0.0036 ±.0003	±18	1.29 ±.06	0.0182 ±.0004	±14	0.0104 ±.0004	±38
42149 (Fig. 3)	3.75 ±.02	–	–	–	3.74 ±.08	78 ±4	0.0043 ±.0015	±21	4.4 ±.2	0.027 ±.001	±27	0.0221 ±.0004	±31
42272[d]	4.37 ±.02	–	–	–	3.3 ±.7	82 ±3	0.0255 ±.0006	±46	–	–	–	0.0327 ±.0004	±59

t_f relative time of fragmentation point
t_{if} relative time of "inverse" fragmentation point (unrealistic solution)
m_f relative percent of mass fragmented at the fragmentation point
σ ablation coefficient
ε_l standard deviation of distances along the fireball trajectory for one measured point
a) the first fragmentation point more important than the second one; only unrealistic "inverse" solution was found
b) terminal mass of the biggest fragment of Lost City fireball from our model: (16 ± 1) kg; splitting trails: see Fig. 5
c) dynamical data available only after t = 2.7 s
d) a great part of systematic time change of residuals left: geometrical position of the trajectory in error?

eral statements on the validity and limitations of our theoretical model.

If the fireball fragments just at a single point and if the precision of the measured distances along the trajectory is better than ±30 m , our method is able to find the fragmentation point (PN 41571 and PN 42149). Precision of ±50 m makes the model hardly usable (PN 42272). Especially if the fragmentation point takes place early on the trajectory (inside the first third), the precision of the observed distances is usually not sufficient to determine the point by our dynamical method (change of velocity is too small).

If the fireball fragmented at two different points, it depends how strong the second fragmentation is relatively to the first. If the second fragmentation is overwhelming, our method can find it (PN 39972, also "inverse" solution exists, but well before the first fragmentation point). If both the fragmentations are of comparable size, our method yields fragmentation point later than the real second fragmentation. At the same time an "inverse" unrealistic solution (adding mass at the "fragmentation" point instead fragmenting it) exists between both the real fragmentation points (PN 41126). If the first fragmentation is stronger than the second one, only the "inverse" unrealistic solution exists (PN 40116). If the fireball fragments at several points, our method finds the most important of them with some preference to later parts of the trajectory caused by greater change of velocity (PN 39404, PN 40590, PN 40617, PN 41327, PN 41963). If "inverse" solutions exist in these cases, they are usually better and somehow summarize influence of all fragmentation points into one fictitious point with adding a good portion of mass instead of fragmentation at several points. *Existence of better "inverse" solution than the normal fragmentation solution indicates the presence of more fragmentation points.* This does not exclude other reasons for "inverse" solutions. *Our method is capable of finding the most important fragmentation point for any fireball for which the precision of the distances measured along the trajectory is better than ±30 m, if it occurred in the second part of the luminous trajectory.* For the first part of the trajectory (namely for the first third) precision should be better than ±10 m, which calls for some new system of recording fireballs.

PN fireballs were mostly measured at centers of dashes between time marks. Remeasuring of exisiting PN records by using

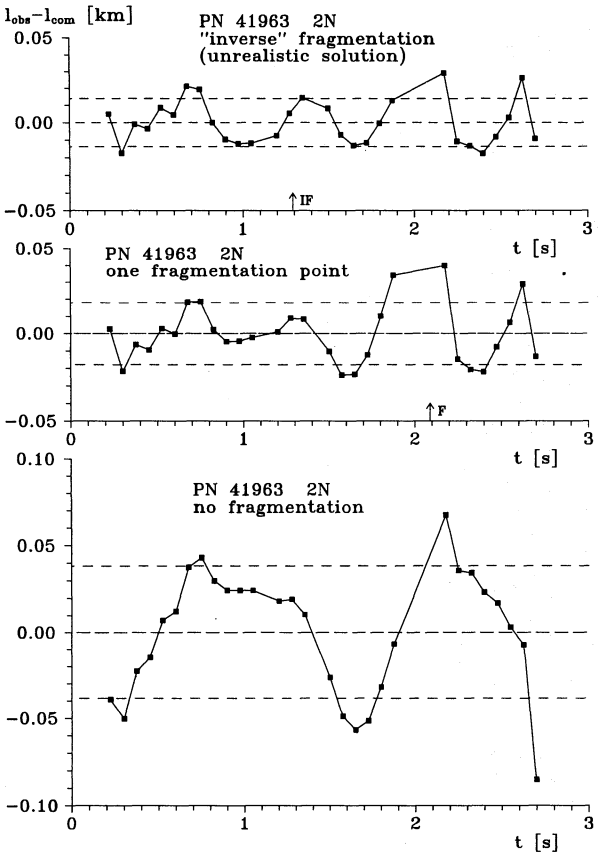

Fig. 7. PN 41963: Comparison of time dependence of residuals from the single body-solution with residuals from our model solution. $l_{com} \equiv l$

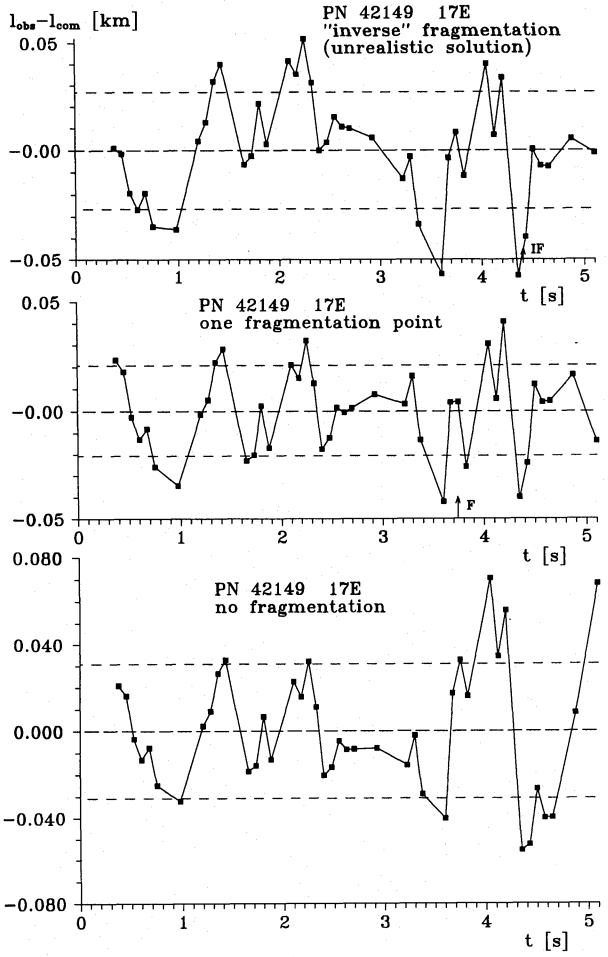

Fig. 8. PN 42149: Comparison of time dependence of residuals from the single body-solution with residuals from our model solution. $l_{com} \equiv l$

the heads of the time marks as reference for the fireball motion may be a simple way of making the precision of distances along the trajectory better.

The main reason for the "inverse" unrealistic solutions seems to be multiple fragmentation. But comparing PN 39404, PN 41571 and PN 42272, we feel that some other reasons may act as well: errors in the geometrical position of the trajectory (we made some tests and the fragmentation solution proved to be quite sensitive to this); influence of the air densities used (we have been using CIRA 72 monthly atmospheres), which may be quite far from the instantaneous air density values; sudden change of velocity at the fragmentation point, which is not included in our model (much higher precision of observations would be also needed to apply such model with sudden velocity changes to observations); and sudden changes of coefficients K and σ, which are assumed constant in our model (namely K may well change due to another meteoroid shape after fragmentation).

3. Application of the model to photographic fireballs

3.1. Classifications

3.1.1. Fragmentation classes

With the results of the preceding section applied to PN fireballs we were able to recognize several different fragmentation classes of meteoroid interaction with the atmosphere:

NF ... without gross-fragmentation (fireballs, which yield only single-body solution with precision $\varepsilon_l \leq \pm 30$ m).

1F ... with one point of overwhelming fragmentation (fireballs, which yielded solution for one fragmentation point with precision $\varepsilon_l \leq \pm 30$ m and for which the "inverse" solution is absent or with worse precision).

MF .. with many points (at least two) of comparable amount of fragmentation (fireballs, which yielded solution for one fragmentation point with precision $\varepsilon_l \leq \pm 30$ m , the "inverse" solution is existing and has better precision than the one-point fragmentation solution).

LA ... low accuracy cases (fireballs with any type of solution, but with precision $\varepsilon_l > \pm 30$ m).

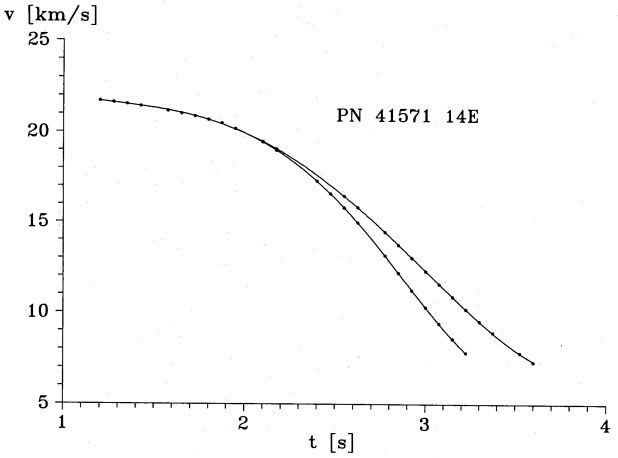

Fig. 9. Velocity dependence on time for PN 41571 fireball as it resulted from our model. The upper curve corresponds to the main body, the lower curve to the biggest fragment, both solved quite independently from their own time marks. Good coincidence of velocity at the fragmentation point proves validity of our model in this case

We applied our model to a sample of 80 records of PN fireballs with precise values of the measured distances and heights. From them 21 proved to be NF class, 19 cases 1F, 11 cases MF and 29 cases were of LA. Thus we have a new tool for classification of such meteoroids for which we have very precise data available, i.e. classification according to their ability to withstand fragmentation and their ability to be then crushed suddenly in the atmosphere at a point. The previous classification of fireballs according to ablation ability (continuous fragmentation included) of their meteoroids into groups (types) I, II, IIIA and IIIB (Ceplecha & McCrosky 1976) and this new classification into NF, 1F and MF classes, they both form two dimensional diagnostic in separating, at least partly, the influence of composition from the influence of structure of the body.

On the other hand, among LA cases we have such a strange event as PN 39828 with no-fragmentation solution of precision $\varepsilon_l = \pm 43$ m, for which we did not find any realistic solution at all, but we found the "inverse" solution with high precision of $\varepsilon_l = \pm 16$ m! The same holds also for independent analysis from the second station record of the same fireball. We suspected geometrical uncertainties as a reason (several degrees difference in inclination of the trajectory to horizon would suffice), but there might be other reasons. Thus we left the final solution to another paper, which will pay attention solely to "inverse" solutions.

3.1.2. Dynamic pressure

We computed the dynamic pressure $p = \rho v^2$ at the fragmentation points of the 1F and MF cases. Histogram of them is in Fig. 10. Preference of some pressure values is evident. Thus we can define several strength categories of fireball meteoroids and determine average values of pressures, at which meteoroid gross-fragmentation takes place:

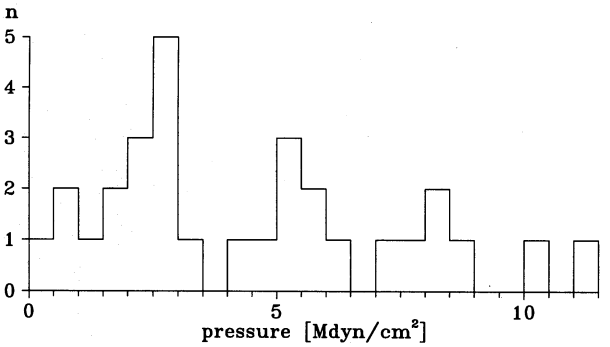

Fig. 10. Histogram of dynamic pressure at fragmentation points of 1F and MF fireballs

strength category	interval of p [Mdyn/cm^2]	average p [Mdyn/cm^2]
a	$p < 1.4$	0.8
b	$1.4 \leq p < 3.9$	2.5
c	$3.9 \leq p < 6.7$	5.3
d	$6.7 \leq p < 9.7$	8.0
e	$9.7 \leq p < 12.$	11.

We also studied the maximum dynamic pressure acting on the NF fireballs. These pressures were mostly below 12 Mdyn/cm^2 with 4 exceptions of very strong bodies, i.e. PN 38737, PN 39521, PN 39775B, which survived as single body up to 15 Mdyn/cm^2 and PN 39935A, which survived up to 50 Mdyn/cm^2.

3.1.3. Ablation coefficient

One of the parameters determined by the model is the ablation coefficient, σ. In principle we have two different values, σ_1 before the fragmentation point and σ_2 after the fragmentation point. For our least squares solutions, it was not possible to leave them both as free parameters: the procedure usually did not converge. The reason for it is a small change of velocity in the first part of the trajectory compared to the second part. Usually the first part of an observed fireball trajectory is equally well fitted inside a very large range of assumed ablation coefficients, while the second part needs a precisely determined value of σ_2; and with this value the first part can also be fitted. Thus the value of ablation coefficient still mostly depends on the later parts of the trajectory, never mind that we compute one value of σ for the entire trajectory. Values of σ before the fragmentation point are usually very uncertain. The value of σ we determined for all 80 studied fireballs is thus really the value σ_2.

Histograms of the ablation coefficients determined for different fragmentation styles are given in Fig. 11. The ablation coefficients for the 1F and MF fireballs sorted into individual groups (I, II, IIIA and IIIB) proved to be smaller than the previously published statistical values (Ceplecha 1988), but quite close to the values derived for NF fireballs. But when the 1F+MF fireballs were computed as NF cases (i.e. as single body, neglect-

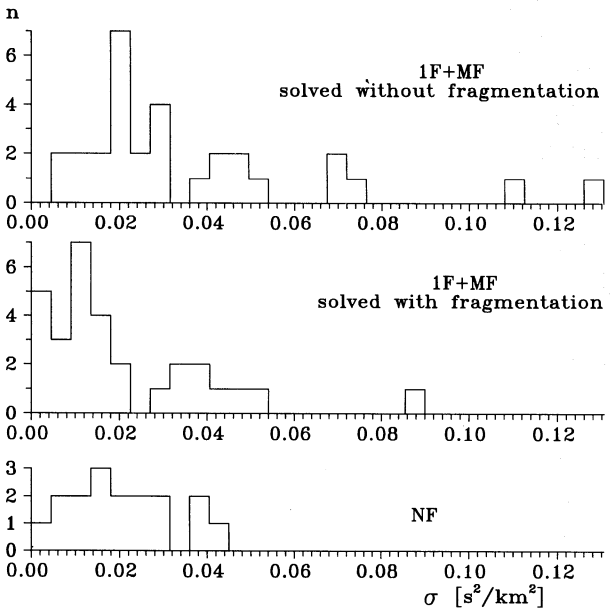

Fig. 11. Histograms of ablation coefficients show the difference between neglecting the gross-fragmentation (top: higher values) and taking it into account in our model (middle: lower values). Genuine NF cases as ascertained by our model (bottom) show similar distribution to the 1F and MF cases (middle)

ing their fragmentation), the values of the ablation coefficients were larger and closer to their previous statistical values. This is one more justification for our model. The resulting average values of the ablation coefficients σ are given in Table 3 for different groups and different fragmentation styles. The statistics are quite small, since we choose only the most precise data available on fireballs. On the other hand, individual values within these statistics are rather precise values disclosing the properties of individual meteoroids.

Table 3 also reveals that the gross-fragmentation is more frequent for stronger types of fireballs. For group I, there are almost twice as many 1F+MF as NF whereas for group II, these two categories occur almost equally. And the only IIIB case we were able to compute with our model is NF. But one should have in mind that the ablation in both single-body and our fragmentation model contains the continuous fragmentation as well. Thus the IIIB type (PN 39973) fragmented only continuously without any sudden gross-fragmentation. The maximum pressure it suffered was only 0.088 Mdyn/cm^2 at the terminal height of 75 km with terminal velocity of 15.5 $\pm$ .3 km/s and with ablation coefficient of 0.59 $\pm$ .02 s^2/km^2; its initial velocity was computed as 16.555 $\pm$ .008 km/s and the bulk density as 0.4 g/cm^3. Other extreme of NF is PN 39935A, a type I fireball, which survived pressure of 50 Mdyn/cm^2 without fragmentation and its very low ablation coefficient 0.0010 $\pm$ 0.0005 guarantees that continuous fragmentation was almost completely absent.

Table 3. Average ablation coefficient σ in s^2/km^2 for different fireball groups (types). n ... number of cases, PSV ... previous statistical values (Ceplecha 1988)

type	n	1F+MF assumed as NF	1F+MF	n	NF	PSV
I	21	0.023	**0.011**	12	0.015	0.017
II	8	0.060	**0.038**	6	0.035	0.041
IIIA	1	0.128	0.088	2	0.15	0.10
IIIB				1	0.59	0.21

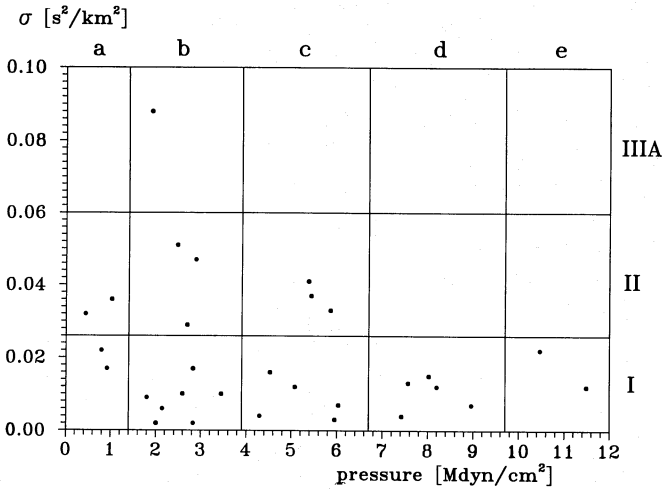

Fig. 12. Ablation coefficient against dynamic pressure at the fragmentation point for 1F and MF fireballs. Each point belongs to one fireball. The grid lines are the dividing lines among different types and categories of fragmenting fireballs (from left to right: a, b, c, d, e; from down up: I, II, IIIA

3.1.4. Two dimensional classification

The two dimensional classification of fireballs is also evident from Fig. 12, where the ablation coefficient σ is plotted against the dynamic pressure at the fragmentation point.

Horizontal lines divide the groups, vertical lines the strength categories. All computed 1F and MF fireballs are presented: the MF cases are all in the group I region, but covering the whole b to e category. Thus the multiple fragmentation is typical for the type I fireballs with $p > 2$ Mdyn/cm^2. About one half of the type I gross-fragmentation is realized at several points for one fireball. Type II fireballs with gross-fragmentation have usually just one fragmentation point. The numbers of cases in different fragmentation styles and for different types of fireballs are given in Table 4.

3.1.5. Bulk densities

Bulk densities can be computed for each fireball individually providing we have a good photometrically determined mass. This statistical material is even less and only quite rough statements can be made. In any case all values of bulk densities

Table 4. Number of cases according to fragmentation styles and fireball types

type	NF	1F	MF
I	12	11	10
II	6	7	1
IIIA	2	1	0
IIIB	1	0	0

computed without fragmentation for 1F+MF cases are significantly lower than when computed with our fragmentation model (for Geminids: see also Ceplecha & McCrosky 1992). On the other hand the bulk density values computed with our model for 17 (1F+MF) fireballs of this study with relevant data come close to the statistical values of bulk densities given in Ceplecha (1988). Thus we feel that our revision of the average ablation coefficients and bulk densities for individual fireball groups does not change the values of the average statistical densities for groups I and II, while it makes the ablation coefficients smaller (Table 3). The reason for this may be the statistical method used for separation of σ from K, because only the product σK was determined from observations in 1976 Ceplecha & McCrosky paper. Thus the statistical values of bulk densities for group I 3.7 g/cm^3 and for group II 2.0 g/cm^3 seem to be close to reality. The one IIIA classification fireball, for which we have computed the bulk density gave almost exactly 0.75 g/cm^3, the statistical value. The one of IIIB classification gave 0.4 g/cm^3, higher than the statistical value, but probably a preferable value, because its photometry was precisely calibrated (rather faint fireball).

Keeping the statistical values of bulk densities given in Ceplecha (1988) and transforming the ablation coefficients according to Table 3, we have a new system of these values closer to reality.

If the same fireball with fragmentation point (1F or MF) is computed like no-fragmentation case (notation: NOF), the ablation coefficient is significantly greater: $\sigma_{1F+MF} = 0.54\sigma_{NOF}$. Admixture of quite a number of fragmentation fireballs dealt with as no-fragmentation cases may be another reason for greater statistical values of ablation coefficients derived in 1976 Ceplecha & McCrosky paper.

3.1.6. Amount of fragmented mass; fragmentation point

Another parameter determined in our model is the amount of fragmented mass, m_f, relatively to the mass immediately before gross-fragmentation. A histogram is given in Fig. 13. The amount of fragmentation for 1F class is typically 60%, which corresponds to breaking the body into approximately two halves with some accompanying small fragments. The second most important value is between 95% and 99%, which corresponds to almost complete disruption of the body. The distribution of m_f for the MF class is more random than for the 1F class. Some preference for 65% is evident. Thus a typical sudden fragmentation for almost half of all fragmented meteoroids is equivalent to stripping away slightly more than half of the mass.

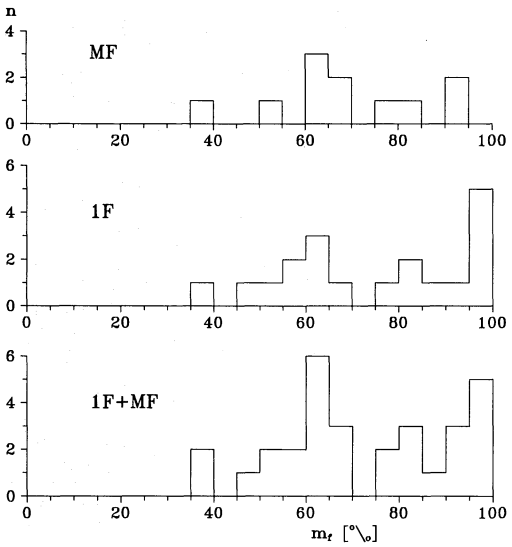

Fig. 13. Histograms of percent of fragmented mass at fragmentation point for 1F and MF fireballs

The position of the fragmentation point on the fireball trajectory is dependent on velocity. With velocities below 15 km/s, the fragmentation point occurs usually during the last second of the trajectory. For velocities over 20 km/s, the fragmentation takes place during the first second of the luminous trajectory. For higher velocities, gross-fragmentation might even cause the onset of lumunosity (see for comparison Geminids with $\approx$ 36 km/s in Ceplecha & McCrosky 1992).

But this question needs more precise observational material, because the changes of velocity at the beginning are small. Study of fainter meteors (small masses) with enough change of velocity at the beginning of the luminous trajectory may be another possibility for understanding this problem.

3.1.7. Initial velocity; dynamic mass

Another parameter determined in our model is the initial velocity. If the same fragmentation fireball (1F or MF) is computed also with the no-fragmentation model (notation: NOF), the change of the resulting initial velocity is the following: the 1F and MF values are either less or greater compared to no-fragmentation (NOF) value of the same fireball. The average relative change $\Delta v_\infty = (v_{\infty(1F \text{ or } MF)} - v_{\infty(NOF)})/v_{\infty(NOF)}$ for all 1F and MF fireballs is -0.0035 with extremes of 0.011 for PN 41963 and of -0.044 for PN 41327. Because the precision of the initial velocities computed from our model is of the order of several units $\times 10^{-4}$, these changes are important for computation of precise orbits of all the 1F and MF cases. The spread of Δv_∞ is large and with not much correlation with any other value (it is -0.007 at v_∞ = 12 km/s and 0.002 at 30 km/s). Thus the only way to derive correct values of initial velocities for orbital

computations is just the application of our fragmentation model for all 1F and MF cases for individual computations of initial velocities. The same also holds for correct initial and terminal masses, which should be therefore determined individually from our gross-fragmentation model.

3.1.8. List of classified fireballs

The list of our final classification of all fireballs we computed follows. It gives PN number of the fireball and classification. The composition group (I, II, IIIA, IIIB) given here is based on our model solutions and may thus differ from statistical classification published for the same fireball before. From our model solutions we better separate type I from type II fireballs using individual σ values.

NF fireballs:
38737 II; 38856 I; 39057 I; 39065 II; 39078 II; 39521A I; 39716B I; 39729C I; 39775B I; 39860C I; 39935A I; 39939 IIIA; 39973 IIIB; 39980A II; 39985A I; 40318A II; 40065B I; 40996 I; 41757 IIIA.

1F fireballs:
38768 bII; 38850 aI; 39000 bII; 39031 bI; 39038B bI; 39055 cII; 39113A bII; 39404 eI; 39479B cII; 39757B bIIIA; 39815 bI; 39820A dI; 39827A bI; 39863A cI; 39878A aII; 40444C aI; 41571 cI; 42149 cI.

MF fireballs:
39775B dI; 39892 cI; 39920 aII; 39962 bI; 40120A bI; 40590 cI; 40617 eI; 41126 dI; 41327 bI; 41963 dI.

LA fireballs:
38737; 38847; 39048; 39060; 39080A; 39755; 39794B; 39828; 39833; 39850; 39856; 39921C; 39988; 39972; 39984B; 40026A; 40116; 40151; 40189A; 40203; 40307A; 40330A; 40353B; 40379A; 40755; 42272.

3.2. Precision of results

3.2.1. Independent results on the same fireball from two stations

We computed 4 fireballs with records of good precision of dynamic data from both stations. Our method was thus applied independently to two records of the same fireball and comparison of the results gave perfect agreement in all 4 cases (Table 5). Fireball PN 39820 is just a borderline case in our classification, but it is more likely 1F class, because the more precise record from station 15W classifies it as 1F. This fireball actually demonstrates differences of results, as we might expect for borderline cases with uncertain classification between 1F and MF.

At this occasion we want to stress that also the NF class cases, when decided on by our model of gross-fragmentation, demonstrate the precision of our model. If 1F or MF cases are dealt with by single body model for the same fireball and the results for two independent records compared, the differences are significantly greater. Except for the more direct indication by time dependence of residuals for any station solution, this disagreement of results is also one of other indications of gross-fragmentation, but only by comparing results from al least two stations.

Table 5. Our model applied to the same fireball with good independent records from both the stations demonstrates in all 4 cases a good feasibility of procedures applied

fireball no. + st.	class	v_∞ [km/s]	σ [s^2/km^2]	m_∞ [kg]	m_E [kg]	ε_l [m]
38856 15E	NF	19.757 ±.006	0.0254 ±.0005	0.036	0.0009	±16
38856 16W	NF	19.751 ±.011	0.0248 ±.0006	0.033	0.0007	±21
39055 8S	1F	16.013 ±.003	0.0469 ±.0005	0.78	0.004	±14
39055 14E	1F	16.017 ±.002	0.0457 ±.0002	0.75	0.005	± 9
39065 16E	NF	17.321 ±.005	0.0303 ±.0005	1.3	0.037	±16
39065 7S	NF	17.343 ±.010	0.030 ±.002	1.2	0.12	±20
39820 14S	MF	24.624 ±.002	0.0147 ±.0006	2.7	0.03	±26
39820 15W	1F	24.644 ±.003	0.0129 ±.0005	2.0	0.02	±23

3.2.2. Lost City fireball; PN data

The Lost City fireball (PN 40590) is a special case of a very long (9 seconds) precisely measured trajectory and with its meteorites recovered (McCrosky et al. 1971). In the course of this work we remeasured the fireball films and recomputed all the data. We also measured all the trails of individual fragments. By intersecting them we determined 3 fragmentation points as given in Table 2. When we applied our method to the whole fireball trajectory we found only the first of them as it is evident from Table 2. But separating the whole trajectory into smaller parts, we were able to find out also the last fragmentation point: then the computed values for the first part containing the first fragmentation point, resulted as $t_f = 5.4 \pm .8$ s, $m_f = 58\% \pm 2$, $\sigma = 0.0142 \pm .0005$ s^2/km^2, $\varepsilon_l = \pm 23$ m; and for the second part as $t_f = 8.2 \pm .5$ s, $m_f = 41\% \pm 2$, $\sigma = 0.0107 \pm .0004$ s^2/km^2, $\varepsilon_l = \pm 23$ m. The fragmented mass at the middle fragmentation point was perhaps too small to be recognized by our model. When we computed with smaller parts of the whole trajectory we, on several occasions, obtained solutions without gross-fragmentation, but in such case the ablation coefficient took over the influence of sudden fragmentation and averaged it over the entire small computed part of the trajectory yielding thus very high values of ablation coefficients (up to 0.6!). After separating the whole trajectory into smaller parts, using our method, and if some of these parts yield solution with a very high value of the ablation coefficient, then the gross-fragmentation point is somewhere inside such a small part. We classified Lost City as MF fireball, the only exception with slightly greater residuals for "inverse" solution than for the normal solution.

Once more: our method is the best for long trajectories with one fragmentation point and with high precision data on distances along the trajectory.

From the point of view of the orbit and of the meteorite falls there is not much change connected with the remeasuring of the Lost City films, but we disclosed one misnumbering of the time marks (breaks of image) at the end of the fireball, which has impact on application of our fragmentation model (for the old interpolation polynomial reduction of velocity data it has very little meaning). We feel that we should publish our work on the newly remeasured Lost City data in more details, which we intend to do in a separate paper.

Also detailed numerical data for each time mark on all 52 fireballs (NF, 1F and MF) computed during the work on this paper, will be published perhaps in some standard format in electronic form. At the moment they are available on floppy disc on request. The same is holding for the PN values of distances, heights, absolute magnitudes and photometric masses for each time mark, which form an ASCII file of slightly over 2 Mbytes.

3.2.3. Precision of fireball film measurements

Method of new measurements of several tens of PN films differ from the method of the "old" measurements. We (Keclíková) measured and used exclusively the heads of the meteor image at each time mark. We also measured by the "old" style for comparison, i.e. centers of dashes (or exceptionally centers of breaks), following the original measurements by Shao. Thus we were able to separate two reasons for differences: method of measurement and the precision of indicator settings. On an average our style of measurement of the image heads proved to be 60% more precise than the measurement of dashes. The reason for this is evidently the wake phenomenon. Also our indicator setting of the Ascorecord measuring instrument together with the automatic PC evaluation proved to be 40% more precise. Thus the results of our new measurements are about twice more precise on an average than the original measurements of the PN films. This is valid for bigger fireballs with well developed wakes, where the definition of the middle of the dash is rather vague.

This invokes a rather fantastic proposal: remeasuring of the PN films, especially bright fireballs with wakes, using the new method and new instrumentation may be quite useful for farther theoretical applications of models similar to the one we present in this paper. In any case our model applied to the old measurements can work with all the intrinsic precision of the "old" data. This may be in some cases 10× more precision in resulting velocity and deceleration data than the values published so far and based on interpolation polynomial solutions (McCrosky et al. 1977). On the other hand the classification of fireballs into NF, 1F and MF classes needs a precision $\varepsilon_l \leq \pm 30$ m: only remeasuring of the PN films can significantly enlarge the number of available records with enough precision for this purpose.

4. Proposal

Generally speaking, with the precision of our photographic fireball data (PN, EN, MORP), we can use only the best records for detailed study of the gross-fragmentation dynamics. For most of these cases, only models with one-fragmentation point give reasonable results. This invokes a proposal for putting into operation some system of cameras with much longer focal distances and sufficiently big field of view. Precision in observed distances along the trajectory should be of the order of several meters. The focal length of the cameras should be around 1 m with large field of view. Such system looks quite fantastic at the moment. But the biggest problem could be the realization of time marks with sufficiently high precision for fireballs photographed with such cameras.

Acknowledgements. We are very much obliged to Dr. Richard E. McCrosky for kindly lending us the PN films for measuring at the Ondřejov Observatory, and moreover to his excellent idea of checking the fragmentation model with theoretically simulated fireballs. Our thanks are due to C.-Y. Shao for his help with searching in the PN archive of the Smithsonian Astrophysical Observatory located at the Oak Ridge Observatory, Harvard, MA, U.S.A. and for his enormous work connected with the original measurements of the PN films. *This work has been supported by grant 30319 from the Czechoslovak Academy of Sciences.*

References

Ceplecha Z., 1988, Bull. Astron. Inst. Czechosl. 39, 221
Ceplecha Z. and Borovička J., 1992, Meteors. In: Benest D., Froeschle C. (eds.) Interrelations between Physics and Dynamics for Minor Bodies in the Solar System, Goutelas 1991, Editions Frontieres, France
Ceplecha Z., McCrosky R. E., 1976, J. Geophys. Res. 81, 6257
Ceplecha Z., McCrosky R. E., 1992, Gross Fragmentation of Meteoroids and Bulk Densities of Geminids from Photographic Fireball Records. In: A.W. Harris and E. Bowell (eds.) Asteroids, Comets, Meteors 1991, Lunar and Planetary Institute, Huston, USA, p. 109
McCrosky R.E., Ceplecha Z., 1969, Photographic Networks for Fireballs. In: Millman P.E. (ed.) Meteorite Research. Reidel, Dordrecht, p. 600
McCrosky R. E., Posen A., Schwartz G., Shao C.-Y., 1971, J. Geophys. Res. 76, 4090
McCrosky R. E., Shao C.-Y., Posen A., 1977, Prairie Network Fireball Data. Center for Astrophysics, Preprint Series Nos. 665, 721
Pecina P., Ceplecha Z., 1983, Bull. Astron. Inst. Czechosl. 34, 102
Pecina P., Ceplecha Z., 1984, Bull. Astron. Inst. Czechosl. 35, 120

This article was processed by the author using Springer-Verlag LaTeX A&A style file version 3.